Micrometer resolved photothermal displacement inspection of optical coatings

E. WELSCH and M. REICHLING†

Physikalisch-Astronomische Fakultät, Friedrich-Schiller-Universität
Jena, Max-Wien-Platz 1, 07743 Jena, Germany
†Fachbereich Physik, Freie Universität Berlin, Arnimallee 14, 14195
Berlin 33, Germany

Abstract. Two-dimensional c.w. photothermal surface displacement (PTD) scans with high spatial resolution provide a new quality for thin-film characterization. This is demonstrated for optical single-layer films of ZrO_2 and MgF_2 on various substrates. Inhomogeneities of the films were detected with a lateral resolution $<2\,\mu m$. Variation of the modulated frequency was employed for depth-profiling. The resolving power has been investigated experimentally and a model for signal generation by absorbing inhomogeneities is presented. A calculation of the photothermal thin-film response for thermally thick coatings is carried out to obtain a better understanding of the PTD images with respect to film absorption and thermophysical sample properties.

1. Introduction

It has been shown that in the field of characterization of optical thin films photothermal methods permit a more detailed investigation of both lateral- and depth-resolved distributions of material inhomogeneities such as absorptive centres in the coating as well as in the substrate [1–3].

There exist three different contactless continuous wave (c.w.) photothermal techniques that are capable of spatially resolved inspection of a sample surface: probe beam refraction (PBR, Mirage-effect), thermoreflectance (TR), and photothermal surface displacement (PTD), i.e. an optical probe of the absorption-induced thermoelastic surface deformation [4–6].

Due to the fact that the PTD response is proportional to the slope of the surface displacement, and because the effect does not need an adjacent medium or a temperature dependent surface reflectivity, both sensitivity and lateral resolution of the PTD technique have been shown to be superior to other techniques [7–9]. The disadvantage, however, is the additional influence of thermoelastic sample properties, whereas TR as well as PBR are mostly governed by the surface temperature and, therefore, are dependent only on optical and thermal material parameters. A PTD scan of the surface will, therefore, produce an image originating from optical and thermal, as well as thermoelastic, inhomogeneities.

The task is to separate both optical and thermophysical properties of the thin film and substrate. This can be achieved by varying the modulation frequency of the heating laser light which, in turn, affects the thermal diffusion length μ_{th}. Depending on whether μ_{th} is large, comparable or small with respect to the film thickness l, the optical and thermophysical inhomogeneities of the film and the substrate can in principle be separated. Uncertainties in the interpretation of the

data can be overcome by calculating the homogeneous thermoelastic (PTD) response for thermally thick and thin films. Such a calculation can at present be performed semi-quantitatively, yielding approximate expressions for the PTD response. In order to interpret the PTD images it is important to estimate the influence of absorption, thermal conductivity, heat capacity, and thermal coefficient of expansion on the photothermal signal. This can be done by properly varying the modulation frequency and, hence, the thermal diffusion length. The ultimate lateral resolution of the PTD technique and its complex amplitude image of an inhomogeneity in thin-film samples must be checked in detail in order to obtain a correlation between the observed images and the structure of the inclusions.

Experimentally we have extended the PTD-technique to measure two-dimensional (2d) images. Combined with a high lateral resolution this provides a powerful tool for analysing thin film inhomogeneities. Scan areas of $2 \times 2\,\text{mm}^2$ have been achieved. Compared to single-line scans these 2d images allow a much superior quality testing of optical thin films. The potential of this technique is demonstrated on single-layer ZrO_2 and MgF_2 films.

It should be emphasized that in contrast to time-dependent measurements frequency domain photothermal experiments should be preferred whenever the sample surface and thin-film response, respectively, is to be measured, i.e. for vanishing influence of the deeper substrate regions. This means that in the high-frequency range, where the heating beam diameter is large compared $\mu_{th} \approx l$, a starving of the thermal information within the heated thin film bulk is avoided [10]. The heat diffusion and expansion process can then be treated approximately in one dimension rather than a full three-dimensional approach, as outlined in the next Section.

2. Calculation of the surface deformation in thin-film samples for high modulation frequencies

In order to estimate the thermoelastic response of thin-film-on-bulk systems, it is necessary to determine both the deformation in the thin-film layer and the backing substrate. To do this, one must solve the thermoelastic wave equations by properly chosen assumptions. They represent a pair of coupled equations describing heat diffusion as well as the thermoelastic response. A practicable way of solving this problem is the treatment of these coupled equations for the related time-independent magnitudes of the temperature T and the scalar elastic potential Φ, respectively.

$$\nabla^2 T - \sigma^2 T = \frac{1}{\kappa} \nabla \cdot \gamma_e, \tag{1}$$

$$\nabla^2 \Phi + \mathbf{k}^2 \Phi = \gamma T, \tag{2}$$

with $\sigma = (1+j)\, 1/\mu_{th}$ (with $j = \sqrt{-1}$ as the imaginary unit) and $\mathbf{k} = \omega/v$ as the thermal and the elastic wave-vector, respectively, and $\gamma = (1+v)/(1-v)\alpha_{th}$ as the thermoelastic coupling factor with α_{th} as the thermal expansion coefficient and v as the Poisson's ratio. The quantities $\mu_{th} = (2\kappa/\rho c \omega)^{1/2}$ and v denote the thermal diffusion length and the longitudinal sound velocity, respectively, with $\alpha = \kappa/\rho c$ as the thermal diffusivity, being the ratio of the thermal conductivity κ and the

heat capacity ρc, and ω as the modulation frequency. The divergence of the incident energy flux is given by

$$\nabla \cdot \gamma_e = -\beta/2 \exp{(\beta z)} I(r),$$

$$I(r) = I_0 \exp{[-(r/R_H)^2]} = \frac{P}{\pi R_H^2} \exp{[-(r/R_H)^2]},$$

(1 a)

assuming an exponential decay of the incident Gaussian beam intensity within the sample material, with β as the absorption coefficient, and R_H the heating beam radius.

The component of the gradient in the z direction (normal to the sample surface, see figure 1) of the elastic potential Φ can be defined as the normal component of the surface displacement

$$U_z(r,0) = \frac{\partial}{\partial z} \Phi(r,0),$$

where

$$2\frac{\partial}{\partial r} U_z(r,0) = \delta\varepsilon$$

(2 a)

is its radial derivative, which is proportional to the measured photothermal deflection angle $\delta\varepsilon$ of the probe beam.

This calculation has been treated in a preceding paper [10] considering the case of moderate modulation frequencies, i.e. restricting the experimental conditions on thermally as well as optically thin films. For this special case, it has been shown that equations (1) and (2) may be solved adequately for the backing only. This means, both the change in temperature and deformation of the thin-film layer itself can be neglected. In other words, only the backing temperature, caused by thin-film as well as substrate absorption β_s and β_B, respectively, acts as the source term in the elastic equation (2) for the backing deformation potential Φ. Hence, in the case of thermally thin films one can restrict the attention to the change in
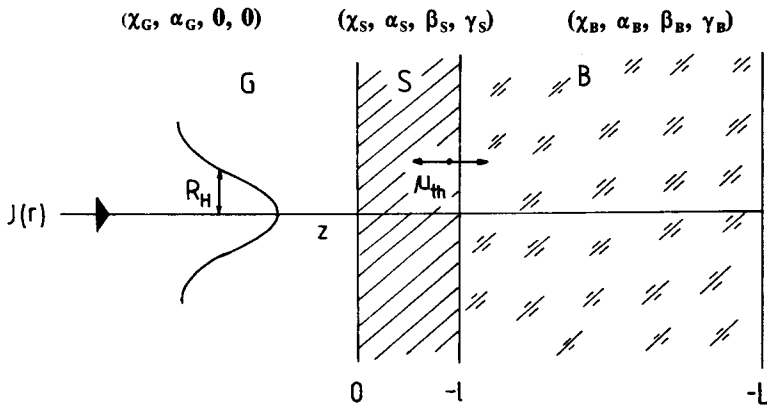

Figure 1. Thermal and thermoelastic two-layer model consisting of an absorbing single layer and substrate of the thickness l and L, respectively. The brackets (κ_i, α_i, β_i, γ_i) containing the thermal conductivity κ_i and diffusivity $\alpha = \kappa_i/\rho_i c_i$, the absorption coefficient β_i and the thermoelastic coupling factor γ characterize the different regions gas (G), single layer (S) and substrate (B), respectively. The sample is presumed to be extending laterally to infinity.

backing temperature and deformation. As an interesting result of the calculation, the photothermal displacement response of a thermally thin film is found to be independent of its thermophysical properties, and especially of its thermal conductivity κ_s.

For a higher modulation frequency range any restriction on the backing response is no longer valid, i.e. in case of thermally thick films the thin-film deformation itself must be taken into consideration, too. Similar to the treatment [10] we solve the equations (1) and (2) by Hankel transformation, but now both Hankel transformations for the temperature as well as the thermoelastic potential in the thin-film layer (t_s, ϕ_s) and the underlying backing (t_B, Φ_B) are performed.

Therefore, the following set of equations must be solved, see figure 1.

$$\frac{\partial^2}{\partial z^2} \phi_s(\lambda, z) - \tilde{k}_s^2 \phi_s(\lambda, z) = \gamma_s t_s, \qquad \text{in} [0, -l] \tag{3}$$

$$\frac{\partial^2}{\partial z^2} \phi_B(\lambda, z) - \tilde{k}_B^2 \phi_B(\lambda, z) = \gamma_B t_B, \qquad \text{in} [-l, -L] \tag{4}$$

with

$$\phi(\lambda, z) = H[\Phi(r, z)]$$

and

$$t(\lambda, z) = H[T(r, z)]$$

as the corresponding Hankel transforms, using the abbreviation $\tilde{k}_{s,B} = \lambda^2 - k_{s,B}^2 = \lambda^2 - \omega^2[(\rho/(\lambda_L + 2\mu_L)]_{s,B}$, the spatial frequency parameter (λ) dependent three-dimensional analogue of the one-dimensional longitudinal elastic wave number $k_{s,B}$. Here, ρ, λ_L, and μ_L denote the mass density, and Lame's constants of elasticity.

The source terms t_s and t_B are obtained by applying a similar Hankel transform on equation (1). It can be shown that $t_s(\lambda, z)$ and $t_B(\lambda, z)$ are the solution to the corresponding one-dimensional thermal problem by only replacing the one-dimensional thermal wave-number $\sigma^2 = 2j/\mu_{th}^2$ by $\sigma^2 + \lambda^2 = \tilde{\sigma}^2$ and the incident intensity by its corresponding spatial intensity spectrum

$$h(\lambda) = H[I(r)] = \int_0^\infty r \, dr \, I(r) J_0(\lambda r) = \frac{I_0 R_H^2}{2} \exp\left[-\left(\frac{\lambda R_H}{2}\right)^2\right]. \tag{5}$$

Therefore, presuming an optically thin and thermally thick single-layer film and a thermally thick substrate with vanishing absorption, i.e. $\beta_B \to 0$ satisfying the relation $(\text{Re} \, \tilde{\sigma})^{-1} < l \ll \beta_s^{-1} \leqslant L$, t_s and t_B may be expressed by

$$t_s(a, z) = h(\lambda) \frac{\beta_s/2\kappa_s}{\tilde{\sigma}_s^2} \exp(\beta_s z), \qquad \text{in} [0, -l], \tag{6}$$

and

$$t_B(a, z) = h(\lambda) \frac{\exp(-\beta_s l)\beta_s/2\kappa_s}{\tilde{\sigma}_s \tilde{\sigma}_B \left(1 + \dfrac{\kappa_s \tilde{\sigma}_s}{\kappa_s \tilde{\sigma}_B}\right)} \exp[\tilde{\sigma}_B(z+l)], \qquad \text{in} [-l, -L), \tag{7}$$

see figure 1 and Appendix A.

For clarity it should be pointed out that equation (3) describes the absorption-induced deformation of the thin-film layer, whereas the influence of the thin film

absorption on the heating and subsequent deformation of the underlying backing is governed by equation (4). Since substrate and thin film are elastically coupled, the surface displacement depends on both the thermoelastic expansion from the backing (B) and the layer (s). For the sake of simplicity let us assume an experimental set-up that ensures free and rigid boundary conditions for $z = 0$ and $z = -L$, respectively, Thus, for a stress-free surface, according to Hooke's law of thermoelasticity [11] the boundary condition

$$\phi_s(\lambda, o) = 0 \qquad (8)$$

must be satisfied, whereas for the deformation-free rear surface from the vanishing component or the displacement normal to the sample surface at $z = -L$ the condition

$$\frac{\partial}{\partial z} \phi_B(\lambda, -L) = 0 \qquad (9)$$

follows. Finally, the stress and displacement continuity conditions at the film-backing interface are explicitly given by

$$\left. \begin{array}{l} \phi_s(\lambda, -l) = \phi_B(\lambda, -l), \\[2mm] \dfrac{\partial}{\partial z} \phi_s(\lambda, -l) = \dfrac{\partial}{\partial z} \phi_B(\lambda, -l). \end{array} \right\} \qquad (10)$$

Now, with the general solution of ϕ_s and ϕ_B, respectively

$$\phi_s = c_1 \exp(\tilde{k}_s z) + c_2 \exp(-\tilde{k}_s z) + h(\lambda) \frac{\beta_s/2\kappa_s}{\tilde{\sigma}_s^2} \exp(\beta_s z) \frac{\gamma_s}{k_s^2 + \beta_s^2 - \lambda^2}, \qquad (11)$$

$$\phi_B = c_3 \exp(\tilde{k}_B z) + c_4 \exp(-\tilde{k}_B z) + h(\lambda) \frac{\exp(-\beta_s l)\, \beta_s/2\kappa_B}{\tilde{\sigma}_s \tilde{\sigma}_B \left(1 + \dfrac{\kappa_s \tilde{\sigma}_s}{\kappa_B \tilde{\sigma}_B}\right)} \exp[\tilde{\sigma}_B(z + l)]$$

$$\times \frac{\gamma_B}{k_B^2 + \sigma_B^2}, \qquad (12)$$

the constants $c_1 \ldots c_4$ of the homogeneous part of the solution are calculable, in principle, using the boundary conditions (8) $\ldots$ (10). In contrast to the calculation procedure for the case of thermally thin films [10], however, we already apply all the assumptions for the low focusing limit:

$$\mu_{\text{th}} < l < R_H \ll \beta_s^{-1} \approx L,$$

i.e. the high-frequency range, at the present stage of the determination of the c_i to ensure an analytical approximation.

Hence, keeping $\tilde{k}/\tilde{\sigma} \approx \lambda/\sigma$, and satisfying equations (8) $\ldots$ (10) we obtain from equations (11) and (12) for the z derivative of the Hankel transform of the surface deformation

$$\frac{\partial}{\partial z} \phi_s(\lambda, 0) \simeq \frac{\partial}{\partial z} \phi_{ss}(\lambda, 0) + \frac{\partial}{\partial z} \phi_{sB}(\lambda, 0) \simeq \gamma_s \frac{\beta_s/2\kappa_s}{\sigma_s^2} \frac{h(\lambda)}{\lambda} + \gamma_B \frac{(\beta_s/2\kappa_s)h(\lambda)}{\sigma_s \sigma_B^2 \left(1 + \dfrac{\kappa_s \sigma_s}{\kappa_B \sigma_B}\right)}. \qquad (13)$$

Obviously, the influence of the backing deformation is described by the second term, whereas the deformation within the thin-film with its response on the surface displacement is governed by the first term of equation (13).

It should be noted that in case of only considering substrate absorption in the analogous limit $\mu_{\text{th}} < R_H < L$ both the Hankel transformation and the related slope of the backing surface displacement shows the same structure as for thin-film deformation $(\partial/\partial z)\,\phi_{ss}(\lambda, \text{o})$, see equation (13). This allows the determination of the purely acting backing signal response and, furthermore the separation of the latter response from that of the thin-film one [8, 10], see Appendix B.

Applying the inverse Hankel transformation and performing an integration according to [12], from equation (13) one can achieve the approximate analytical expression for the surface displacement $U_z(r, \text{o})$ and its radial derivative, respectively, the latter being proportional to the complex valued photothermal displacement signal:

$$
\left.
\begin{aligned}
\frac{\partial}{\partial r}\, U_{z_s}(r, \text{o}) &= \frac{\partial}{\partial r}\, H^{-1}\!\left[\frac{\partial}{\partial z}\, \phi_s(\lambda, \text{o})\right] = \frac{\delta}{\partial r}\, U_{z_{ss}}(r, \text{o}) + \frac{\partial}{\partial r}\, U_{z_{sB}}(r, \text{o}) \\[2ex]
&= -\gamma_s \frac{\beta_s/2\kappa_s}{4\pi}\, \sqrt{\pi} P_0 \exp\left(-j\pi/2\right) \left(\frac{\mu_{\text{th}_s}}{R_H}\right)^2 \left(\frac{r}{R_H}\right) \\[2ex]
&\quad \times \sum_{\nu=0}^{\infty} \frac{\Gamma(3/2+\nu)/\Gamma(3/2)}{\nu!(\nu+1)!} \left(-\frac{r^2}{R_H^2}\right)^{\nu} \\[2ex]
&\quad + \gamma_B \frac{\beta_s/2\kappa_B}{2\sqrt{2}} (\mu_{\text{th}_B})^2 \mu_{\text{th}_s} \frac{1}{1+\left(\dfrac{\kappa_s \rho c_s}{\kappa_B \rho c_B}\right)^{1/2}} \exp\left(-j\frac{3\pi}{4}\right) \frac{\partial}{\partial r}\, I(r),
\end{aligned}
\right\} \quad (14)
$$

with

$$
\frac{\partial}{\partial r}\, I(r) = -\frac{2}{R_H}\left(\frac{r}{R_H}\right) I(r).
$$

From equation (14) we may conclude as an interesting result that because of $\mu_{\text{th}}^2/\kappa \simeq (\rho c)^{-1}$ the surface displacement slope is dependent on the thermal conductivity of the thin film material only via the thermal influence of the thin-film layer on the backing temperature. (This influence is now bulk-like and therefore not so small as for thermally thin-film samples, as shown previously [10].) The κ dependence in the thin-film contribution itself, however, is cancelled out. This behaviour may be elucidated by physical reason in this two component thermally thick thin-film sample configuration taking into account that the deformation in the thin film is caused by a bulk absorption and subsequent heating, whereas the backing deformation originates from the heat flux across the film-backing boundary and is therefore governed also by the thin-film thermal conductivity κ_s via its effusivity $\sqrt{\kappa_s(\rho c)_s}$ and thermal diffusion length μ_{th_s}, respectively.

The proportionality of the surface displacement slope to γ_s, γ_B, and β_s, and the modulation frequency as well as phase lag course, on the other hand, would be expected.

Finally, let us estimate the ratio or the first and second term of equation (14) for the maximum slope, i.e. at $r = r_{max}$

$$\frac{\dfrac{\partial}{\partial r} U_{z_{ss}}(r_{max}, o)}{\dfrac{\partial}{\partial r} U_{z_{sB}}(r_{max}, o)} \simeq f(R_H, \omega) \frac{\gamma_s}{\gamma_B} \frac{(\rho c)_B}{(\rho c)_s} \left(\frac{R_H}{\mu_{th_s}}\right). \tag{15}$$

Here, the corrective factor $f(R_H, \omega)$ is of the order of magnitude of 1, which is calculable numerically. Assuming that γ_s, γ_B and $(\rho c)_B$, $(\rho c)_s$ respectively, are nearly of the same order of magnitude for dielectric coatings on optical substrates the ratio will be governed by R_H/μ_{th_s}. (This assumption does not hold in general.)

For typical photothermal thin-film investigation in the high-frequency region, the relation

$$R_H \approx 40 \ldots 10 \mu_{th}(\omega_1) > l > \mu_{th}(\omega_2)$$

is valid, where ω varies commonly from a few $100\,Hz$ (ω_1) up to several MHz (ω_2) [9]. In case of dielectric thin films, however, the upper frequency limit to reach a thermal diffusion length of the order of magnitude of the thin-film thickness is often given already in the $10\,kHz$ region. This is caused by a considerable decrease of the thermal conductivity for some dielectrics in thin-film format compared to that in bulk [9, 14].

Hence, taking into consideration that the above calculated approximation becomes relevant for $R_H > l > \mu_{th}$ it can be concluded from expression (15) that the dominant part in the high-frequency range is the thin-film deformation component $\partial/\partial r \, U_{z_{ss}}(r, o)$. Note that this result holds in contrast to the case of thermally thin films, where the thin-film contribution itself to the overall surface displacement response is shown to be negligible [10]. It should be emphasized that, despite the approximative character of the calculation in the low focusing limit, both vertical and lateral components of the thermal expansion are taken into account, see Appendix C. This is illustrated by the fact that the thin-film surface displacement slope $\partial/\partial r \, U_{z_{ss}}(r, o)$ is broadened compared to the corresponding temperature profile, see equations (6), (13) and (14), respectively. Therefore, for modulation frequencies corresponding to thermal diffusion lengths $\mu_{th} \gg l$ or $\mu_{th} \ll l$ neither the thermal conductivity of the backing nor that of the thin-film coating itself influences the surface displacement response of the sample considerably, but the signal is mainly governed by thin-film absorption and thermal expansion of the substrate and the film, respectively.

In conclusion, performing photothermal surface displacement measurements on thin-film-on-substrate-samples, the signal of thermally thick, optically thin films will be determined by thin-film absorption coefficient β_s rather than by thin-film absorption $\beta_s l$ and thermal conductivity κ_s, respectively. Furthermore, for $\mu_{th} < l < R_H$ the response is dependent on thermal expansion γ and heat capacity ρc in the same manner as for $R_H > \mu_{th} > l$ by only replacing the backing quantities by those of the thin-film material [10]. In the transition range $\mu_{th} \approx l$ a numerical solution instead of equations (13) and (14) is needed [13].

3. Experimental

C.w. photothermal displacement measurements are well established methods for bulk and thin-film material characterization in the frequency range from $10\,Hz$
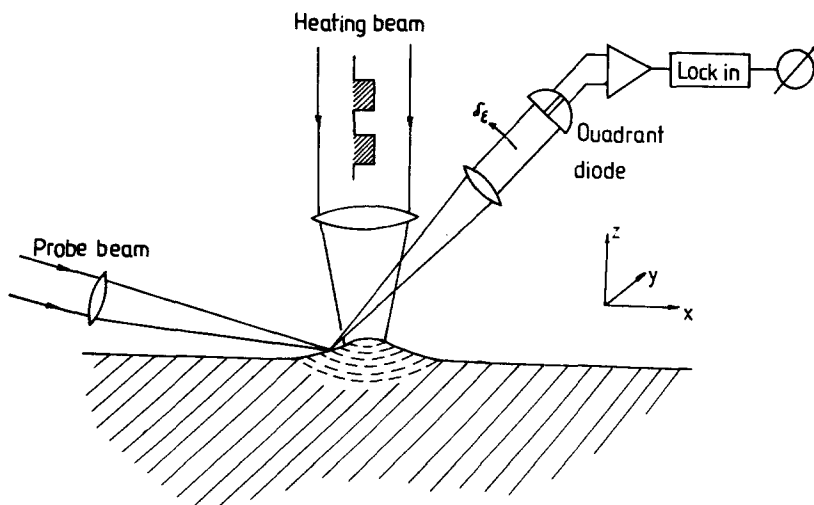
Figure 2.   Experimental set-up.

to 10 MHz [6–9, 15–17]. We used an experimental set-up similar to that commonly used and described in detail elsewhere [6, 9, 18], as illustrated in figure 2. The sample is periodically heated by an acousto-optically modulated Ar^+ ion laser, which provides the heating beam. The heating beam is reflected by a movable mirror to allow adjustment to maximum signal and then focused on to the sample surface. The time-dependent temperature rise produces a deformation bulge rising and falling with the chopper frequency. The surface displacement is detected by a He–Ne laser, which acts as the probe beam and is fixed at an incident angle of about 45°. The probe beam is reflected at the surface and the deflection from the initial reflectance angle (i.e. without displaced surface) is measured by a quadrant photodiode detector consisting of four segments of photodiodes separated by small spacings. The deflection angle $\delta\varepsilon$ results in a change of relative intensities on the segments and, hence, provides information about the displacement at the sample surface. According to equation (2 a) it can be assumed, that $\delta\varepsilon$ is proportional to the radial derivative of the surface displacement, normal to the sample surface. The signal is obtained by taking the difference between the diode segment signals in x and y direction, i.e. the two possible, independent directions of the probe beam deflection in the incident plane of the probe beam and perpendicular to it can be measured separately. After detection the signal is processed by a two channel vector lock-in amplifier. Thus, amplitude and phase of the PTD signal can be recorded directly. During measurements the offset between heating and probe beam is kept at fixed value of maximum signal. The arrangement allows a two dimensional (x, y) point-by-point raster scanning of the sample surface, generating photothermal amplitude and phase images.

    The lateral resolution of the measurements may be defined as the minimum distance between two measured (x, y) positions of a detectable contrast (i.e. an optical, thermal or thermoelastic inhomogeneity), which are separable from each other leading to different image points and, thus, unambiguously characterizing the photothermal structure under investigation.

From the nature of thermal waves a microscopic imaging necessarily works in the near field limit. Therefore, the intrinsic resolution is dependent on the depth as well as the geometry of a detected inhomogeneity rather than the thermal wavelength $\lambda_{th} = \mu_{th} 2\pi$, but instrumentally limiting factors such as heating beam and probe beam spot size and the step size of the scanner must also be considered.

On the other hand, by using high-quality translation stages with a repetition reproducibility better than $0.1\,\mu m$ the pixel size (i.e. the squared translation step width) can be chosen to be smaller than the probe beam spot size. In the next Section it will be proved experimentally that, through the scanning procedure, an ultimate lateral resolution can be reached, which is given by a step width in the order of a few microns rather than by the thermal diffusion length, and the probe beam waist of some 10 microns and the heating beam waist of about 40 microns, see e.g. figures 6, 7, and 8.

According to the aim of our investigation the depth sensitivity in the z direction of the measuring procedure must be also considered briefly. To do this it can be pointed out that for sufficient high modulation frequencies, in accordance to equation (15) the displacement signal of optical thin-film-on-bulk samples is governed by film properties only. A numerical solution of equations (3) and (4) performed by Reichling *et al.* [9, 13] confirms this result quantitatively. However, it should be emphasized that a simple scanning in thickness direction by changing the modulation frequency and, hence, the thermal diffusion length, as shown in case of photoacoustic gas-cell-microphone technique (or related photothermal methods, which measures directly or indirectly the change in surface temperature) cannot be expected by performing photothermal surface displacement technique [16]. This is caused by the additionally acting thermoelastic response creating, at least, the surface deformation.

4. Resolving power and signal interpretation in PTD microscopy

Before presenting the experimental results of the (x, y) resolved PTD scanning at the surface of selected dielectric single-layer films deposited on optically highly transparent substrates the ultimate lateral resolution of the apparatus has been checked. To do this an integrated circuit (IC) structure was chosen, which can be imaged by both PTD technique and by optical microscopy. Results are given in figure 3 (a)–(d) showing a detail of a rectangularly shaped edge of the structure PTD images $(a$–$c)$, and are compared by the optical imaging (d) by reflection microscopy. The edge was imaged photothermally with different magnification, see figure 3 (a) 1 pixel $\triangleq 10\,\mu m$, 3 (b) 1 pixel $\triangleq 4\,\mu m$ and 3 (c) 1 pixel $\triangleq 2\,\mu m$, respectively.

Note that the performed PTD operation mode that measures the probe beam deflection in the x direction, prefers the image contrast quality of an extension of the structure in the y direction. Obviously, it is seen from the amplitude image in figure 3 (c) that, caused by the Gaussian shaped probe beam intensity distribution, the step-wise scanning of the conducting edge yields a better spatial resolution than that which is given by the probe beam waist of about 10 microns (taken at the e^{-2} points). Furthermore, originating from the fact the surface region close to the conducting stripe is also illuminated by the heating beam, a signal smaller than that of the stripe region will be observed at the edge boundary. The thermal broadening in case of $R_H \approx \mu_{th}$, however, is of the order of a few microns [10],
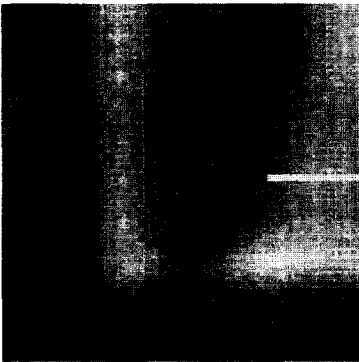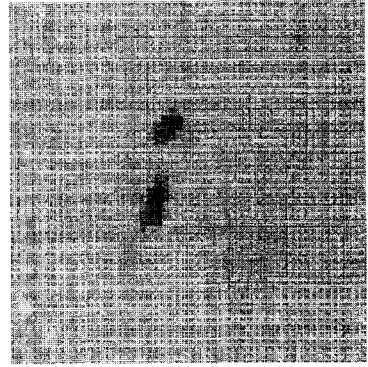
(a)

(b)
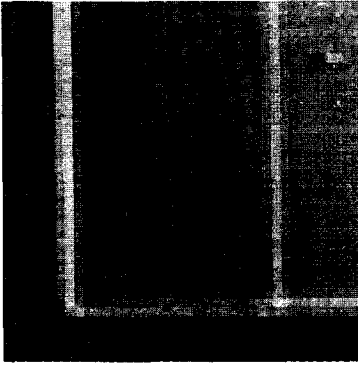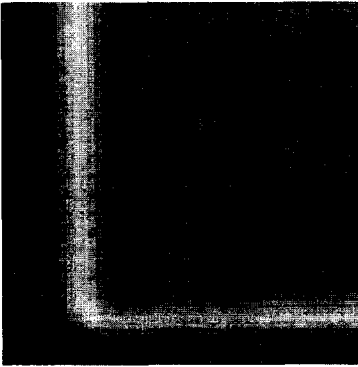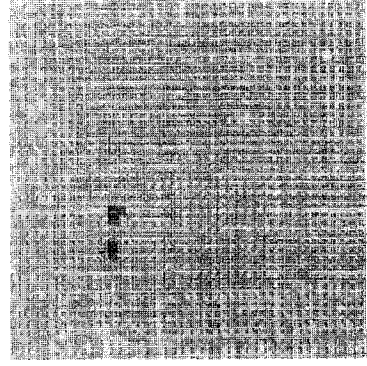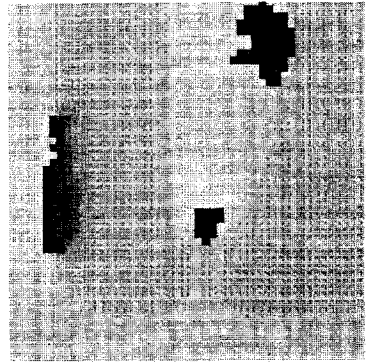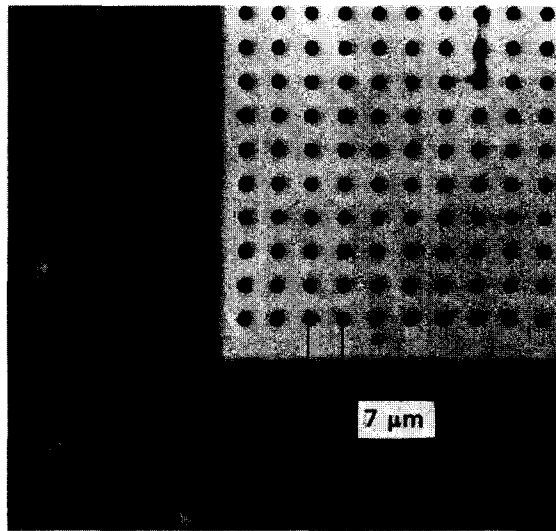

(c)

(d)

Figure 3. Amplitude image of an edge of a conducting stripe in an IC structure using PTD technique (a) ... (c) and optical reflection microscopy (d). The PTD images represent the probe beam deflection in the x direction, i.e. in the incident plane on the probe beam, for different magnification.

hence, demonstrating the favourable lateral resolution power of the PTD technique compared to other photothermal techniques.

The situation is further complicated by the different reflectivities in the stripe region and close to it leading to a change in incident intensity of the heating beam as well as that of the probe beam reflected by the IC surface, and, therefore, also influencing the imaging.

Exploiting the photothermal information of the thin-film samples completely, given not only by amplitude but also by phase images, the measured PTD response must be considered more carefully. Figure 4 shows the PTD image of an area of $200 \times 200\,\mu m$ of a 2λ optical thickness ZrO_2 film on a BK7 substrate for frequencies of 1 kHz (a) and 10 kHz (b). The observed inhomogeneities typically occur as pair-like structures in the amplitude, in some cases accompanied by either a jump of π in the phase image. Furthermore, the extension of the imaged inclusion decreases for higher frequency indicating that the corresponding inhomogeneity is situated at least partially beneath the substrate surface or at the film–substrate interface.

To explain these experimental findings it must be pointed out that the inhomogeneities may be considered as strongly absorbing inclusions acting as the origin of regions of enhanced photodisplacement [19]. The related extension varies from a few up to some tens of microns, their absorption peak relative to the lowest absorption in regions without inclusions is changed by a factor of 5 up to 100.

Caused by the PTD measuring technique the probe beam is directed at the flank of the deformation bulge normally at the point of the maximum slope. Hence, assuming an inclusion of sufficient absorptivity, the nearly Gaussian shaped heating intensity at the $(1/e^2)$ distance $\simeq R_H$ can exceed that of the centre of
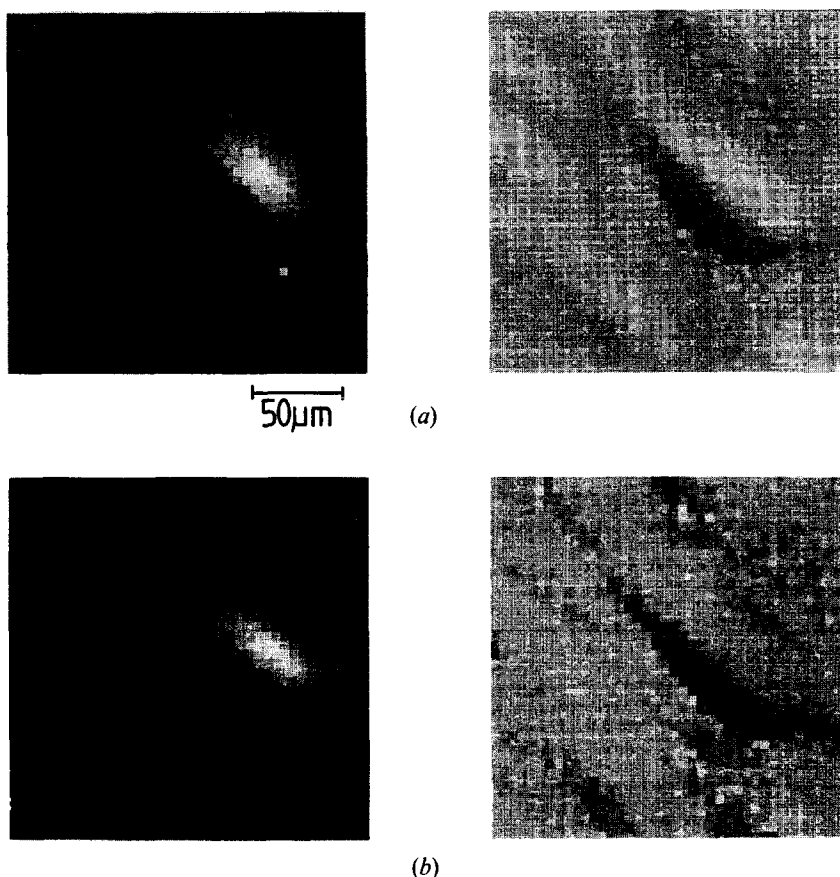
Figure 4.   PTD amplitude (left) and phase (right) image of the 2λ $ZrO_2/BK7$ sample. Fixed area of $200 \times 200\,\mu m$ $(a) \simeq 1\,kHz$, $(b) \simeq 10\,kHz$.

the heating. Thus, satisfying the condition: pixel size $<$ PB waist and size of the inhomogeneity, respectively, according to figure 5 a displacement profiling by the PB will be simulated.

Note that, in general, the inclusion is not extended rectangularly with respect to the scanning direction. Additionally, the rise or fall of the absorptivity in the scanning direction may be assumed to be smoothed rather than given by a jump or edge-like structure, thus distorting the typical slope according to figure 5 (c). Nevertheless, the distance d between the extrema can be roughly estimated as the size, i.e. the related linear extension of a strongly absorbing inhomogeneity. The asymmetry, arising in principle, however, connected with a jump in phase of π will be observed, when the absorbing inhomogeneities (IHs) exceed the basic absorption of the thin film by more than a factor of 10, see figure 4, where the shadowed PTD scanning image is seen excellently.

5.   Imaging of ZrO_2 and MgF_2 single-layer films

For frequency resolved ZrO_2 images, see figure 4, a decreased extension of the absorbing sites against frequency has been concluded. In contrast to this fact let us
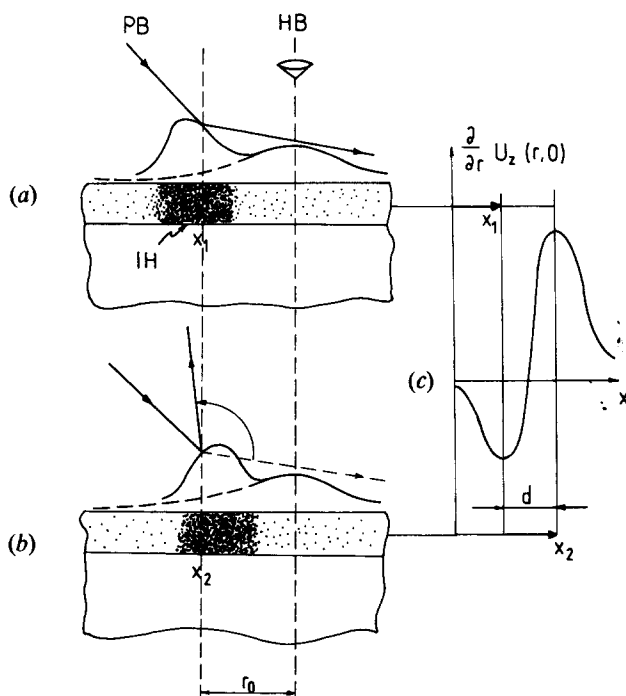
Figure 5. Signal peculiarities by sample scanning in x direction over an inhomogeneity (strongly dotted area) with compared to the basic drastically increased absorption, keeping a fixed offset r_0 between probe beam (PB) and heating beam (HB). (a) negative slope of the PTD amplitude at the right flank of the absorbing inhomogeneity (IH) (position x_1), crossing zero and reaching (b) a positive slope at the left flank (position x_2), accompanied by a jump of π of the phase caused by the quadrant photodiode detection technique. (c) qualitative PTD amplitude response by scanning over an absorbing IH.

consider figure 6, showing an inhomogeneity of about 50 microns (a) at 1 kHz and, magnifying a detail of the upper boundary region by a factor 4 at 1 kHz (b) and 40 kHz (c). From figure 6, however, it follows that for the MgF_2 coatings no significant decrease of the extension of the absorbing inclusion with increasing modulation frequency could be observed. Furthermore, a set of ZrO_2 and MgF_2 thin films with different film thickness have been also investigated in the frequency range of 1 kHz up to 100 kHz confirming the above results and showing that not only size but also density of inclusions per unit area is diminished for ZrO_2, but remains nearly constant in case of MgF_2 films. This results from the difference in thermal properties of ZrO_2 and MgF_2 thin films [4, 15, 20]. For the given modulation frequency the ZrO_2 film is thermally thick, and therefore the resulting signal is described by equations (14), (15), while this does not hold for MgF_2. Details will be discussed in [19]. Hence, the PTD response in case of ZrO_2 films will be governed by the thin-film absorption coefficient β_s rather than by the related thermal conductivity κ_s, but not in case of MgF_2 films. Therefore, a decreased inclusion density against frequency is indicating that the absorption inhomogeneities are situated at the film-substrate interface or beneath the substrate surface.
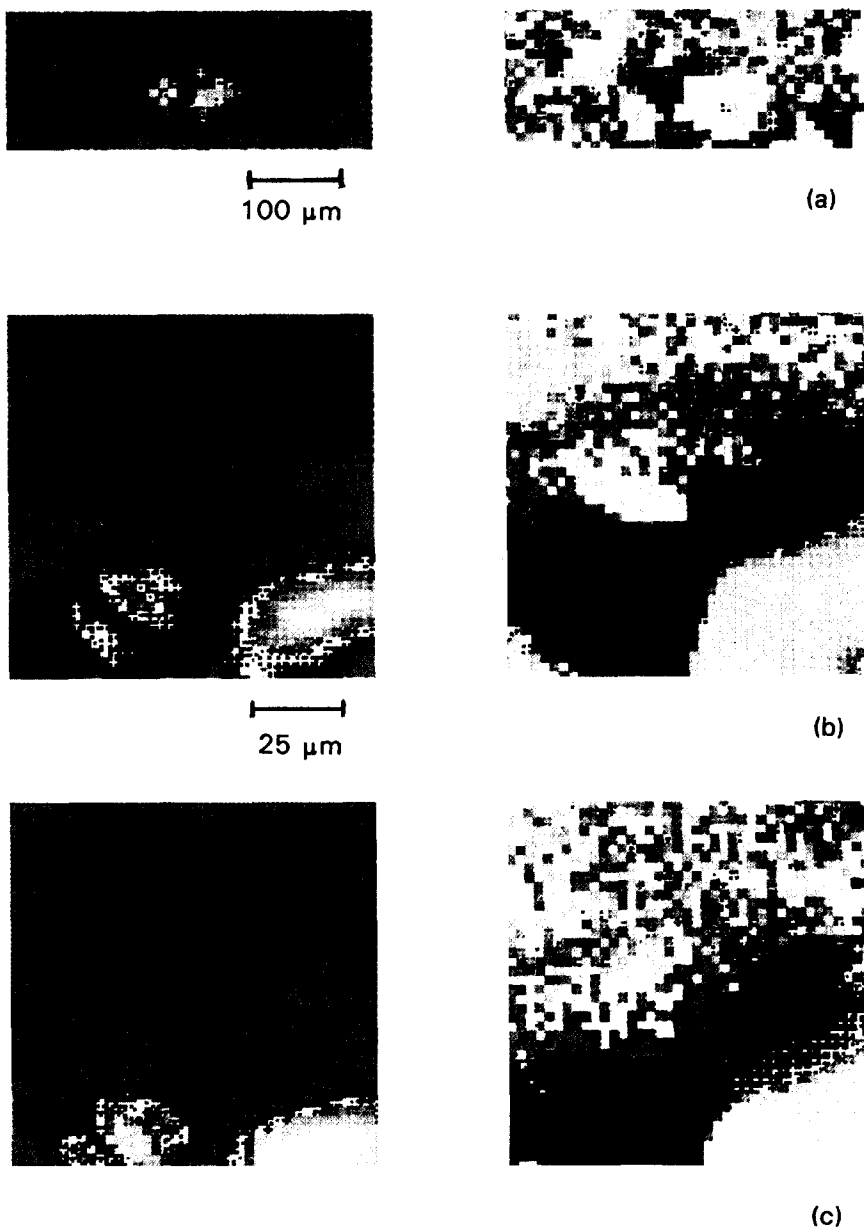
100 µm   (a)

25 µm   (b)

(c)

Figure 6.   PTD amplitude (left) and phase (right) image of the $\lambda/2$ $MgF_2/BK7$ sample
    showing a strongly absorbing absorption site (a) at 1 kHz and (b), (c) an upper
    boundary region magnified by the factor of 4 at 1 KHz (b), 40 kHz (c), respectively.

Next, figure 7 shows a strongly absorbing inclusion within the λ MgF_2 thin
film on quartz, demonstrating both profiling in the amplitude and π jump in the
phase image, respectively. According to figure 5 and the statement in Section 4,
from this microscopical image an extension of about 30 microns can be estimated.
    A final demonstration of the capability of the spatially resolved PTD image
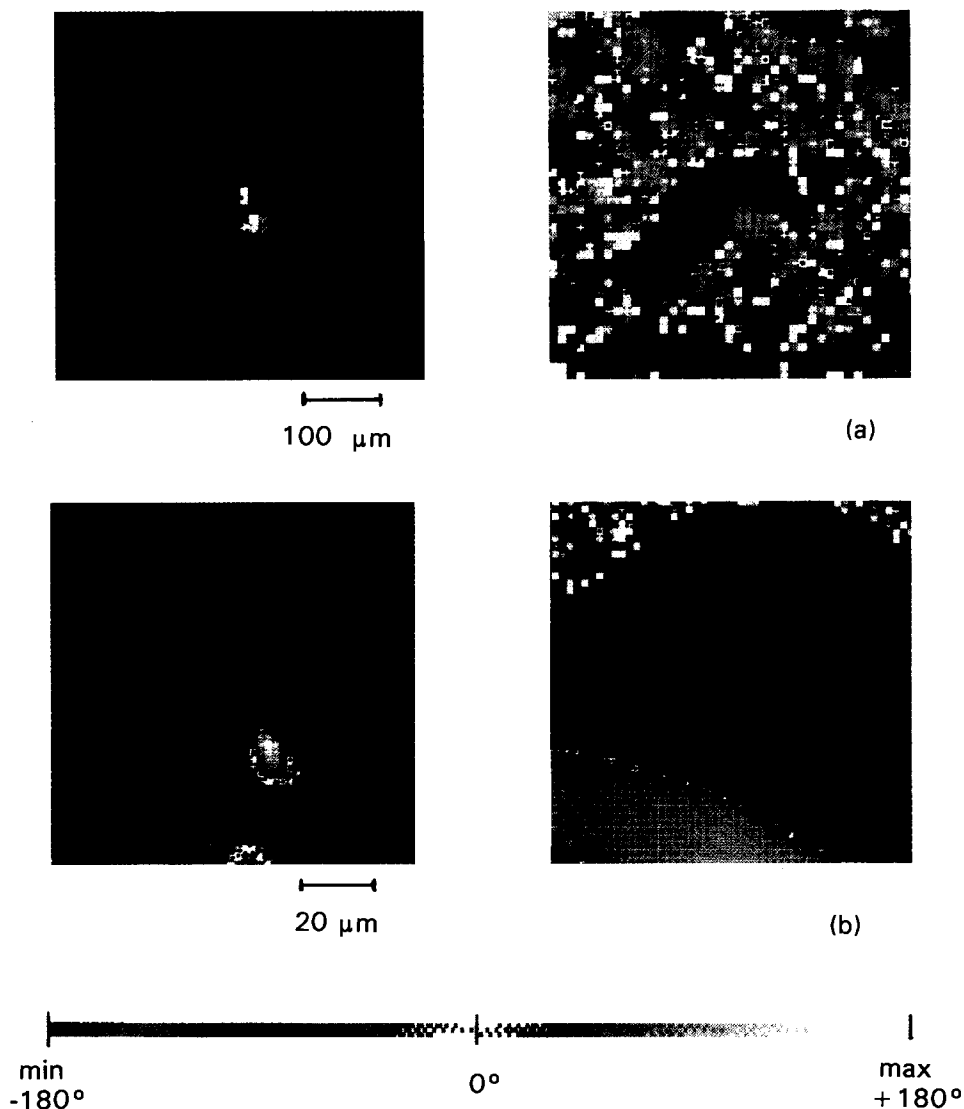analysis is given by figure 8 showing the transition from moderate to high

100 μm (a)

20 μm (b)

min   0°   max
-180°   +180°

Figure 7.   PTD amplitude (left) and phase (right) image of the λ MgF$_2$/quartz sample
       showing a strongly absorbing site at 1 kHz (a) situated in an area of 500×500 μm, (b)
       magnified by factor of 5.

resolution. A selected IH in the $\lambda/2$ MgF$_2$ film on MgF$_2$ substrate of about 40
microns extension is characterized by three different magnifications, satisfying
successively the conditions PB waist < pixel size < IH diameter (no profiling, but π
jump) (a), and pixel size < PB waist, IH diameter (profiling as well as π jump) (b),
(c). In figure 8 (c) a pixel size of 1·25 microns has been used marking both ultimate
lateral (x, y) resolution and feasibility of the PTD 2d sample surface scanning
technique for an inspection of dielectric thin-film coatings with high spatial
resolution, only choosing appropriately the experimental parameters like modula-
tion frequency, the diameter of the Gaussian probe as well as heating beam and the
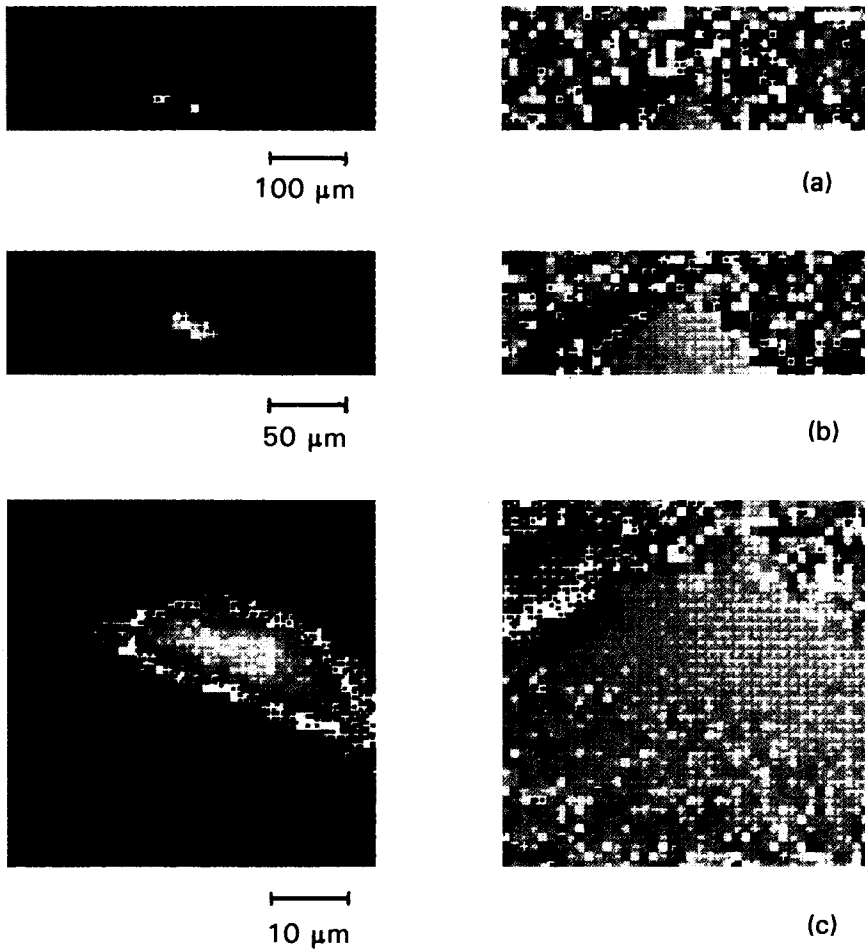scanning step width (i.e. the pixel size). ·

Figure 8. PTD amplitude (left) and phase (right) image of the $\lambda/2$ MgF_2 on MgF_2 sample, absorption IH below within an area of $500 \times 500\,\mu m$ (*a*), magnified by 2 (*b*) and 10 (*c*), respectively, at 1 kHz.

6. Conclusions

The peculiarities of the photothermal surface displacement technique with respect to a spatially and frequency resolved characterization of optical thin-films have been treated to some extent showing how an uncertainty, i.e. a more sophisticated interpretation of the experimental data, which may occur in this technique, can be removed.

To do this, first the calculation of the thermoelastic response has been extended to the case of thermally thick optical films on a substrate. With the help of this theory, the influence of both film absorption as well as thermophysical properties and experimental parameters on the photothermal images can be estimated.

Second, a carefully performed experimental investigation of the sample surface scans depending on size and jump of microscopical inhomogeneities, probe and

heating beam profile, and step width (pixel size) has been shown to be also necessary.

Although, initially, our interest was mainly focused on checking the surface displacement technique as an appropriate method of the measurement and interpretation of weak, localized thin-film absorption losses, it was also thought that our experimental results do reflect some interesting details for the optical thin-film community. Any optical coating optimization is shown to be dependent on the correlation between optical losses, thermal properties, thin-film microstructure, coating design, deposition technique, and a better understanding of the fundamental laser damage mechanisms. For instance, such a $2d$ sample surface absorption mapping is of importance, when the origin of the radiation breakdown has to be investigated. Any correlation between the absorbing inhomogeneity (IH) density and the damage statistics would be an indication of the thermal origin of the considerably differing laser damage resistivity over the sample surface. (It should be noted that, at least, with respect to the thermally induced damage, it is not of importance whether the photothermal response is caused by absorptive IH or by thermoelastic IH.)

Furthermore, some of the ideas and intuitions should be also of interest for future non-destructive photothermal inspection of non-optical films such as functional coatings.

Acknowledgments

Appendix A

Similar to equations (2), (3) and (4) in Section 2 the heat diffusion equation (1) leads to:

$$\frac{\partial^2}{\partial z^2} t_G(\lambda, z) - \left(\lambda^2 + \frac{j\omega}{\alpha_G}\right) t_G(\lambda, z) = 0, \qquad \text{of } [0, +\infty], \qquad (A1)$$

$$\frac{\partial^2}{\partial z^2} t_S(\lambda, z) - \left(\lambda^2 + \frac{j\omega}{\alpha_S}\right) t_S(\lambda, z) = -\frac{\beta_s}{2\kappa_s} h(\lambda) \exp(\beta z), \qquad \text{of } [0, -l], \quad (A2)$$

and

$$\frac{\partial^2}{\partial z^2} t_B(\lambda, z) - \left(\lambda^2 + \frac{j\omega}{\alpha_B}\right) t_B(\lambda, z) = \frac{\beta_B}{2\kappa_B} h(\lambda) \exp[\beta_B(z+l)], \qquad \text{of } [-l, -L], \quad (A3)$$

with

$$\tilde{\sigma}_{S/B}^2 = \lambda^2 + \frac{j\omega}{\alpha_{S/B}}$$

see figure 1. Again, the Hankel transformation has been used. The general solution

for the regions G, S, B, respectively, are:

$$t_G = \overline{c_1} \exp(\tilde{\sigma}_G z) + \overline{c_2} \exp(-\tilde{\sigma}_G z), \qquad \text{of } [0, +\infty], \tag{A4}$$

$$t_s = \overline{c_3} \exp(\tilde{\sigma}_s z) + \overline{c_4} \exp(-\tilde{\sigma}_s z) + \frac{\beta_s/2\kappa_s}{\tilde{\sigma}_s^2 - \beta_s^2} h(\lambda) \exp(\beta_s z), \qquad \text{of } [0, -l], \tag{A5}$$

$$t_B = \overline{c_5} \exp[\tilde{\sigma}_B(z+l)] + \overline{c_6} \exp[-\tilde{\sigma}_B(z+l)]$$

$$+ \frac{\beta_B/2\kappa_B}{\tilde{\sigma}_B^2 - \beta_B^2} h(\lambda) \exp[\beta_B(z+l)], \qquad \text{of } [-l, -L]. \tag{A6}$$

The constants $\overline{c_1}$ and $\overline{c_6}$ are zero because of the thermally thick regions G and B, the other constants are calculable using the following boundary conditions:

$$t_G(\lambda, 0) = t_S(\lambda, 0), \tag{A7}$$

$$t_S(\lambda, -l) = t_B(\lambda, -l), \tag{A8}$$

$$\kappa_G \frac{\partial}{\partial z} t_G(\lambda, 0) = \kappa_S \frac{\partial}{\partial z} t_S(\lambda, 0), \tag{A9}$$

$$\kappa_S \frac{\partial}{\partial z} t_s(\lambda, -l) = \kappa_B \frac{\partial}{\partial z} t_B(\lambda, -l), \tag{A10}$$

representing the continuity conditions for the temperature and the heat flux at the boundary $z = 0$ and $-l$, respectively.

Presuming an optically thin and thermally thick single-layer film and a thermally thick non-absorbing substrate ($\beta_B \to 0$), i.e. (Re $\tilde{\sigma}_{S,B})^{-1} < l \ll \beta_S^{-1} \lesssim L$ from the equations (A4)–(A10) it follows:

$$t_S(\lambda, z) = h(\lambda) \frac{\beta_s/2\kappa_s}{\tilde{\sigma}_S^2} \exp(\beta_s z), \qquad \text{of } [0, -l], \tag{A11}$$

$$t_B(\lambda, z) = h(\lambda) = \frac{\exp(-\beta_S l)\, \beta_s/2\kappa_s}{\tilde{\sigma}_S \tilde{\sigma}_B \left(1 + \frac{\kappa_S \tilde{\sigma}_S}{\kappa_B \tilde{\sigma}_B}\right)} \exp[\tilde{\sigma}_B(z+l)], \qquad \text{of } [-l, -L] \tag{A12}$$

$\sim$ equations (6), (7) in Section 2.

Similarly, the pure thermal bulk response of an weakly absorbing substance can be derived for vanishing film thickness for equations (A4), (A6) in case of $(\text{Re}\,\tilde{\sigma}_B)^{-1} \ll L \ll \beta_B^{-1}$ using the boundary conditions:

$$t_G(\lambda, 0) = t_B(\lambda, 0), \tag{A13}$$

$$\kappa_G \frac{\partial}{\partial z} t_G(\lambda, 0) = \kappa_B \frac{\partial}{\partial z} t_B(\lambda, 0). \tag{A14}$$

We find:

$$t_B(\lambda, z) = \frac{\beta_B/2\kappa_B}{\tilde{\sigma}_B^2} h(\lambda) \exp(\beta_B z), \tag{A15}$$

in correspondence to the thermally thick film, see equation (A11).

Appendix B

In the absence of the overlayer; instead of equations (3) and (4) of Section 2

$$\frac{\partial^2}{\partial z^2}\,\varphi_B(\lambda,\,z)-\tilde{k}_B^2\varphi_B(\lambda,\,z)=\gamma_B t_B(\lambda,\,z), \qquad \text{of } [0,\,-L], \tag{B1}$$

is valid, with t_B according to equation (A15).

The general solution φ_B is given by:

$$\varphi_B=c_5\,\exp\,(\tilde{k}_B z)+c_6\,\exp\,(-\tilde{k}_B z)+h(\lambda)\,\frac{\beta_B/2\kappa_B}{\tilde{\sigma}_B^2}\,\exp\,(\beta_B z). \tag{B2}$$

The constants c_5 and c_6 are found using the boundary conditions:

$$\varphi(\lambda,\,0)=0, \tag{B3}$$

$$\frac{\partial}{\partial z}\,\varphi(\lambda,\,-L)=0, \tag{B4}$$

instead of equations (8)–(10) of Section 2.

In the limit, $\mu_{th}\ll R_H<L<\beta_B^{-1}$,

$$\frac{\partial}{\partial z}\,\varphi_B(\lambda,\,0)=\gamma_B\,\frac{\beta_B/2\kappa_B}{\sigma_B^2}\,\frac{h(\lambda)}{\lambda} \tag{B5}$$

is found [10].

Therefore, according to equations (13) and (14) of Section 2 the ratio of thin film and bulk surface displacement is approximately given by:

$$\frac{\dfrac{\partial}{\partial r}\,U_{zS}(r,\,0)}{\dfrac{\delta}{\partial r}\,U_{zB}(r,\,0)}\simeq\frac{\gamma_S}{\gamma_B}\,\frac{(\rho c)_B}{(\rho c)_S}\left(\frac{\beta_S}{\beta_B}\right). \tag{B6}$$

This result holds in contrast to thermally thin optical films on substrates, where this ratio will be only determined by $\beta_S l/\beta_B R_H$ rather than by thermophysical properties [8, 10]. Because of $\beta_S/\beta_B\gg1$ the assumption of neglected substrate absorption, see Appendix A, which is justified in many cases for thermally thin films, holds more than ever for thermally thick films.

Appendix C

Using cylindrical coordinates, from equation (2) of Section 2 it follows:

$$\frac{1}{r}\,\frac{\partial}{\delta r}\left(r\,\frac{\delta\phi}{\partial r}\right)+\frac{\partial^2}{\partial z^2}\,\phi+k^2\phi=\gamma T. \tag{C1}$$

Neglecting both radial components of the deformation and the inertia term, equation (C1) can be simplified by:

$$\frac{\partial^2}{\partial z^2}\,\phi=\frac{\partial}{\partial z}\,U_z\simeq\gamma T, \tag{C2}$$

and

$$\frac{\partial}{\partial r} U_z(r, 0) \simeq \frac{\partial}{\delta r} \gamma \int_0^L T(r, z)\, \mathrm{d}z. \tag{C 3}$$

This means, that a solution is to be sought which summarizes the vertical contributions of the thermoelastic deformation, but neglects any lateral expansion. To show that the approximation performed in Section 2 is less crude, we consider the surface displacement slope caused by thin-film deformation in the low focusing limit $\mu_{\mathrm{th}} < l < R_{\mathrm{th}}$. From equation (6) of Section 2 there follows by inverse Hankel transformation:

$$\frac{\partial}{\partial r} U_z(r, 0) \simeq -\gamma \frac{\beta_S / 2\kappa_S}{\sigma_S^2} \int_{-l}^0 \mathrm{d}z \exp(\beta_S z) \int_0^\infty \mathrm{d}\lambda\, h(\lambda) J_0(\lambda r) \lambda^2 \tag{C 4}$$

$$\simeq -\gamma \frac{\beta_S l}{4\kappa_S} \mu_{\mathrm{th}s} 2 \exp\left(-j\frac{\pi}{2}\right) \frac{\partial}{\partial r} I(r), \tag{C 5}$$

and:

$$U_z(r, 0) \simeq \gamma \langle T(r, z)\rangle_z L, \tag{C 6}$$

respectively. Hence, the surface displacement slope follows the heating beam profile, and the displacement itself results from the average temperature labelled by the brackets.

Thus, any lateral acting thermal expansion is cancelled out, in contrast to the treatment of Section 2 and Appendix B, equation (B1), where the corresponding Hankel transformed equation has been solved. (Note that the subscript B must be replaced by S in order to treat the thin film case.) Obviously, as seen from equation (B 5) of Appendix B and [10], this solution incorporates also lateral thermal expansion and, thus, describes the thermophysical process more precisely.

References

[1] ABATE, J. A., SCHMID, A. W., GUARDALBEN, M. J., SMITH, D. J., and JACOBS, S. D., 1985, *Laser Induced Damage in Optical Materials*, edited by H. E. Bennett, D. Milam, A. H. Guenther, B. E. Newnam, *NBS Spec. Publ.*, **688**, 385.

[2] ABATE, J. A., and ROIDES, R., 1988, *J. Phys., Colloque C6*, **44**, 497.

[3] SCHMID, A., SMITH, D., GUARDALBEN, M., and ABATE, J., 1984, *Proc. SPIE*, **476**, 136.

[4] FOURNIER, D., BOCCARA, A. C., and BADOZ, J., 1979, *Digest of topical meeting on photoacoustic spectroscopy* (Washington, D.C.: OSA) paper ThA1; BOCCARA, A. C., FOURNIER, D., JACKSON, W. B., and AMER, N. M., 1980, *Optics Lett.*, **5**, 377.

[5] ROSENCWAIG, A., OPSAL, J., SMITH, W. L., and WILLENBORG, D. L., 1985, *Appl. Phys. Lett.*, **46**, 1013.

[6] AMER, N. M., 1983, *J. Phys. Colloque C6*, **44**, 185; AMER, N. M., OLMSTEAD, M. A., KOHN, S., FOURNIER, D., and BOCCARA, A. C., 1983, *Appl. Phys.* A, **32**, 141.

[7] WELSCH, E., WALTHER, H. G., ECKARDT, P., and TON LAN, 1988, *Can. J. Phys.*, **66**, 638.

[8] WELSCH, E., WALTHER, H. G., FRIEDRICH, K., and ECKARDT, P. J., 1990, *J. Appl. Phys.*, **67**, 6575.

[9] REICHLING, M., WU, Z. L., WELSCH, E., SCHAEFER, D., and MATTHIAS, E., 1992, *Springer Series in Optical Sciences*, Vol. 69, edited by D. Bicanic (Berlin, Heidelberg: Springer).

[10] WELSCH, E., *J. mod. Optics*, **38**, 2159.

[11] CHADWICK, P., 1964, *Progress in Solid Mechanics*, vol. 1, edited by I. N. Sneddon and R. Hill (Amsterdam: North-Holland), Chap. VI, p. 274.

[12] RYSHIK, J. M., and GRADSTEIN, J. S., 1963, *Tables of Series, Products and Integrals* (Berlin: Deutscher Verlag der Wissenschaften).

[13] REICHLING, M., and GRÖNBECK, H., 1993, *J. appl. Phys.* (submitted).

[14] RISTAU, D., and EBERT, J., 1986, *Appl. Optics*, 25, 4571.

[15] OPSAL, J., ROSENCWAIG, A., and WILLENBORG, D. L., 1983, *Appl. Optics*, 22, 3169.

[16] MANDELIS, A., WILLIAMS, A., and SIU, E. K. M., 1988, *J. appl. Phys.*, 63, 92.

[17] BALAGEAS, D. L., BOSCHER, D. M., DEOM, A. A., and ENGUEHARD, F., 1990, *Proceedings European Conference on Thermophysical Properties*, Vienna, (to be published in High Temperatures-High Pressures).

[18] MUNIDASA, M., and MANDELIS, A., 1992, *Photothermal Imaging and Microscopy, Progress in Photothermal and Photoacoustic Science and Technology*, edited by A. Mandelis (Amsterdam: Elsevier), vol. 1, p. 299.

[19] WELSCH, E., REICHLING, M., SCHÄFER, D., and KAISER, N., 1993, *Appl. Optics* (submitted).

[20] LAMBROPOULOS, J. C., JOLLY, M. R., AMSDEN, C. A., GILMAN, S. E., SINICROPI, M. J., DIAKOMIHALIS, D., and JACOBS, S. D., 1989, *J. appl. Phys.*, 66, 4230.